Development of Single- and Multi-Hole Fast Response Pressure Probes for Turbomachinery Applications

J. F. Brouckaert

von Karman Institute for Fluid Dynamics
Turbomachinery Department
72, Chaussée de Waterloo
B-1640 Rhode-St-Genèse
Belgium

ABSTRACT

This contribution focuses on the progress made in the development and use of fast response pressure probes at the Turbomachinery Laboratory of the von Karman Institute.

Over the last three years, substantial efforts have been invested into the development of a new fast response 3-hole pressure probe with a characteristic dimension of 3.0 mm. The particular features of the probe are the hybrid probe geometry (cylindrical front and elliptical rear body), the use of miniature silicon piezoresistive sensors implemented in the same plane underneath the probe surface, the rectangular shape of the pressure holes, to improve spatial resolution and frequency response, and the use of base bleed intended to reduce dynamic errors due to vortex interactions on unsteady pressure and flow angle.

Additionnally, two other single-sensor probes have been designed and manufactured : a Ø 2.5 mm probe combining a pneumatic total pressure tap and a 12.5 μm half-shielded thermocouple with the fast response sensor and a miniature Ø 1.5 mm probe also combining a pneumatic total pressure tap with the fast response sensor.

The paper addresses the various steps of the probe design and manufacturing of these probes. Static and angular calibrations are then described as well as the characterization of the dynamic response from shock tube experiments. Data processing methods are proposed and first applications in a transonic turbine stage are presented.

NOMENCLATURE

Roman

C	chord [m]	
Cp	pressure coefficient [-]	
K	calibration coefficient [-]	
O	offset [V]	
P	pressure [bar]	
S	sensitivity [V/bar]	
T	temperature [K]	

Greek

α	incidence angle [°]	
ε	absolute error	
γ	pitch angle [°]	
θ	angular position [°]	
ρ	density [kg/m^3]	
φ	yaw angle [°]	

Subscripts

ax	axial
tot	total conditions
dyn	dynamic pressure
r	rotor
0	central or total conditions
L	left
M	Mach number
R	right
S	static
T	total

INTRODUCTION

The importance of unsteady flow phenomena inside turbomachines has no longer to be demonstrated. The proof of it is the progress made over the last decades in both numerical and experimental fields towards the complete time-resolved three-dimensional analysis of compressible flows.

However, the accurate measurement of the flow field parameters like unsteady pressures and temperatures, flow angles and turbulence levels still remains an important

engineering problem. As a matter of fact, turbomachinery flows are characterized by high levels of unsteadiness due to blade passing frequencies up to several tens of kHz. Moreover, the size and geometry of the rotating and non-rotating blade passages lead to highly three-dimensional flows and require good spatial resolution of the measurement techniques used.

The present paper concentrates on the development of single- and multi-sensor pressure probes designed for the accurate measurement of unsteady flow angle and velocity vector. Fast response pressure probes have the advantage of offering a high analogue bandwidth, a high signal-to-noise ratio, and a good reliability and robustness as compared to hot-wire techniques for instance. In addition to the flow velocity vector, aerodynamic probes also indicate the total and static pressure as time-resolved quantities.

Three decades have passed since the first attempts were made to convert conventional pneumatic probes into a faster response device thanks to the advent of semiconductor pressure transducers. Since then, many researchers of different laboratories have developed various types of fast response probes, ranging from the simple fast response Pitot probe to complex four- or five-hole aerodynamic probes. Various philosophies were followed regarding probe geometries but over the years, and along with the evolution of piezoresistive sensors, lots of efforts were invested in probe miniaturization and increase of bandwidth. For a detailed and comprehensive review of fast response pressure probe development, the reader is referred to the recent papers of Sieverding *et al.*, 2000; Kupferschmied *et al.*, 2000; or Ainsworth *et al.*, 2000.

Still, space and time resolution remain important issues and progress has to be made towards more accurate measurements, namely by understanding and correcting dynamic errors affecting aerodynamic probes.

MULTI-SENSOR PROBE

The development of fast response pressure and temperature measurement techniques at the von Karman Institute has been driven mainly by the use of a large short duration annular turbine cascade facility (Sieverding & Arts, 1992) converted into a full stage transonic turbine test rig in 1994 operating at engine simulated Reynolds and Mach numbers.

One of the main objectives for the development of a fast response 3-hole pressure probe was therefore to measure the time-resolved velocity vector at the outlet of the turbine stage, where the associated blade passing frequencies are of the order of 7 kHz.

Probe Design

Many important aspects have to be considered in the design process of fast response aerodynamic probes. The geometry and size of the probe are intimately linked to aerodynamic and mechanical constraints that often result in very conflicting requirements. Moreover, it is very difficult to dissociate the influence of size and geometry on the steady and unsteady characteristics of a probe, which makes the design even more complex.

The minimal probe size for highest spatial resolution will be determined by the size and the number of sensors to be implemented in the probe head. Time resolution will also be affected through the size and location of the pressure holes whereas blockage effects and velocity gradient errors have to be minimized as well.

The probe geometry is mainly dictated by aerodynamic constraints through static considerations which are linked to the steady state characteristics of the probe (angular range and sensitivity, Mach and Reynolds number sensitivity, etc.) and through dynamic considerations linked in turn to unsteady flow phenomena around the probe which will induce dynamic errors on the time-resolved measurements (dynamic stall, circulation induced lift, added mass effects or von Karman vortex interactions).

Concept.

In the light of the above mentioned considerations and with the view on applications to turbomachinery, a probe concept was established in which the following objectives were set :
- three piezoresistive sensors would be implemented in the same measurement plane in order to minimize three-dimensional effects on pressure readings.
- reduction of dynamic errors in order to avoid unsteady signal corrections.
- protection of the sensors by sub-surface mounting and probe robustness in view of industrial applications.

The result of the long and iterative design process is presented in Figure 1 as a front and cross-sectional view of the VKI AP3-H30 fast response three-hole probe.
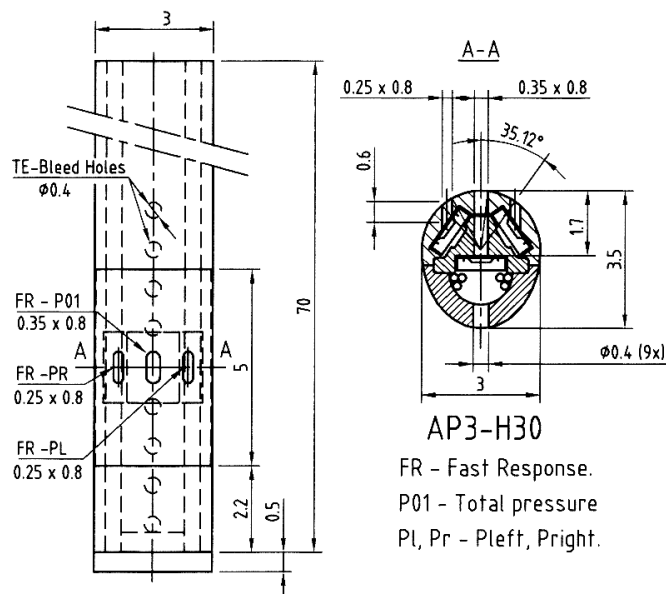

Figure 1. *The VKI AP3-H30 fast response 3-hole pressure probe.*

The particular features of the AP3-H30 probe are the hybrid probe geometry (cylindrical front and elliptical rear body), the use of miniature silicon piezoresistive sensors implemented in

the same measurement plane underneath the probe surface, the rectangular shape of the pressure holes to improve spatial resolution and frequency response, and the use of base bleed intended to reduce dynamic errors due to vortex interactions on unsteady pressure and flow angle. AP3-H30 stands for *Aerodynamic Probe* with *3 sensors*, *Hybrid shape* of *3.0* mm characteristic dimension.

The whole design process has been the topic of a previous paper (Brouckaert *et al.*, 1998.) but will be briefly summarized hereafter.

Hybrid Geometry.

The choice of a hybrid probe geometry was discussed on the basis of steady state flow field computations around several profiles. Two different geometries were considered in the early stages of the probe development. A circular profile, which is known to be the least sensitive to dynamic errors (namely no dynamic stall effects nor circulation induced lift), and an elliptic profile, which provides an increased rigidity for an identical blockage (a 3.0 mm width by 4.0 mm length ellipse has an inertia which is twice the inertia of a Ø 3.0 mm circle). A comparison of the pressure and Mach number distributions around both profiles clearly showed the advantage of a cylindrical front shape as regards yaw angle measurements.

Piezoresistive Sensors.

The sensors used are Endevco 29682 - 15 Psi absolute piezo-resistive pressure sensors (Figure 2). Their dimensions are 1.68 mm length by 1.22 mm width and 0.3 mm height. Their diaphragm natural resonance frequency is of the order of 180 kHz and their temperature range is –54°C/+121°C. A particularity of their design is the sculptured diaphragm for stress concentration for an improved pressure sensitivity (24 to 47 mV/V/bar). The sensors are powered at 5 Volts DC by an electronic circuit incorporating an indirect sensor temperature measurement by a sense resistor in series with the sensor bridge and of equal overall resistance. Additionally to the bridge output voltage, this arrangement delivers a sense voltage proportional to the sensor temperature which is used in a post-test numerical correction for temperature effects on sensitivity and offset (Ainsworth *et al.*, 1994).
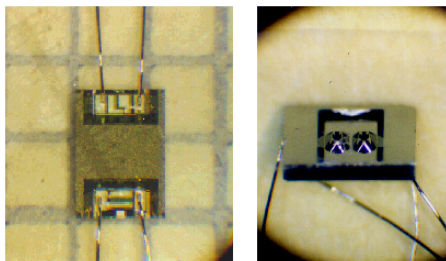

Figure 2. *Endevco 29682-15 Psia sensors with sculptured diaphragm for stress concentration.*

Frequency Response.

The yaw angle sensors are mounted 0.6 mm underneath the surface while the arrangement of the total pressure sensor in the same plane requires this sensor to be moved back, leaving a 1.7 mm long hole between the sensor and the cylinder surface (Figure 1).

Calculating the frequency response of the total pressure line following the theory of Bergh & Tijdeman, 1965, results in a frequency response of 36 kHz for a hole of 0.35 mm diameter.

However, rather than using a circular hole, rectangular holes were chosen following calculations by Richards, 1986, who demonstrated that the frequency response of non-circular tubes is equivalent to circular tubes with an equivalent diameter $d_{eq} = 4 \times$ (cross section area)/(length of perimeter).

Replacing the circular hole of 0.35 mm diameter by a rectangular hole of 0.35×0.8 mm increases the frequency response from 36 to 42 kHz, the equivalent diameter being 0.5 mm. Similarly, the yaw angle holes are rectangular slots of 0.25 x 0.8 mm, which brings the equivalent diameter to 0.4 mm with a corresponding frequency response of 82 kHz.

Dynamic Errors.

Among unsteady effects causing dynamic errors, unsteady lift variations and dynamic stall do not exist for cylindrical probes with circular cross section. However, as the chosen hybrid profile is asymmetric, unsteady lift induced errors are present although expected to be small. Considering the angular position of the separation points (C_f=0 at θ=82°) from 2D steady N-S simulations, incidence variations of more than ± 8 degrees are needed before the separation point is displaced on the rear elliptical body.

On the contrary, wake induced dynamic errors resulting from the upstream effect of vortex shedding in the probe trailing edge region are expected to be important. Moreover, a phenomenon called "lock-on" can occur in some cases where the shedding frequency synchronizes itself with a harmonic component of the blade passing frequency, resulting in even higher measurement errors.

Base Bleed.

A possibility to reduce or even eliminate the effect of these parasite pressure fluctuations, is to stabilize the wake by blowing air through the probe trailing edge. Considering the area of the internal passage for the blowing air mass flow, blowing holes of d=0.4 mm spaced at l/d = 2.5 and covering a length of 3 probe shaft diameters were chosen.

An extensive programme of water tunnel flow visualizations by ink ejection orifices on a 10/1 probe model and by laser sheet method confirmed the beneficial effect of base bleed on the wake vortical structure. The blowing effect results in the formation of two smaller and separate vortex streets. The vortices of smaller size and strength induce therefore reduced pressure fluctuations on the front part of the profile.

A quantitative study by means of 2D unsteady Navier-Stokes simulations was then performed to complement the qualitative results from visualizations. The objective was to determine to which extend the pressure fluctuations would be reduced on the profile as well as the influence of base bleed on the steady state pressure distribution. As shown in Figure 3, the blowing results in strongly attenuated pressure fluctuations up to the leading edge, whereas the time-averaged pressure distribution

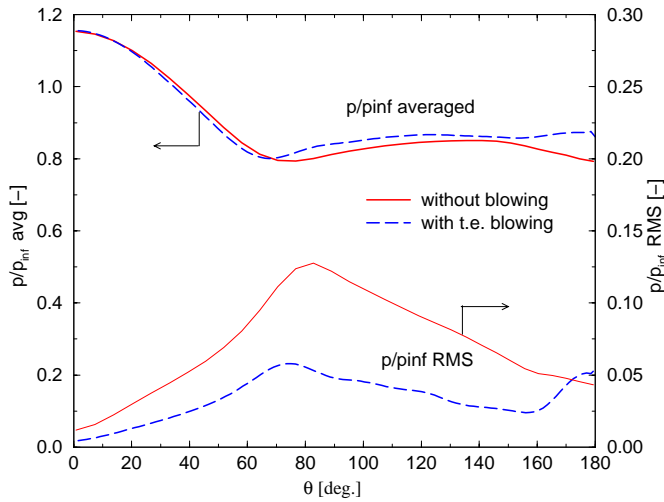is only slightly modified and hardly affected in the front part of interest.

Figure 3. *Time averaged pressure distribution and fluctuating pressure component (RMS) on hybrid profile, $Ma_\infty=0.43$, $Re_d=15000$, from 2D unsteady N-S computations.*

These results are translated in terms of error on the unsteady yaw angle in Figure 4 where the angular sensitivity was calculated on the basis of the average pressure distributions of Figure 3.
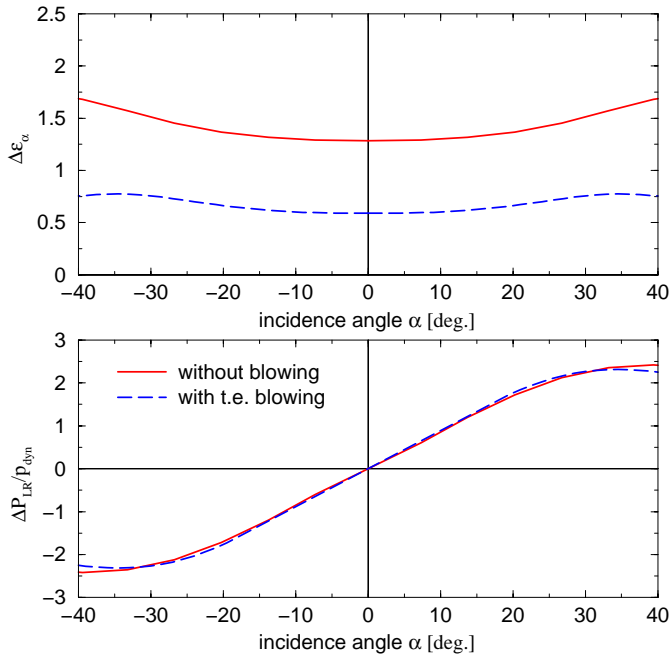

Figure 4. *Reduction of yaw angle error due to trailing edge blowing (up). Angular sensitivity calculated from the computed average pressure distributions (down).*

The error was computed using only the RMS values of pressure at any incidence angle. It can be clearly seen that the smallest error caused by these fluctuations is already higher

than ± 1.3 ° (at zero incidence). This value is reduced to ± 0.6 ° in the case of blowing and substantially lower over the whole angular range of interest.

The investigation of an optimum blowing rate was then performed experimentally through wind tunnel tests on a 2/1 circular model instrumented with semiconductor sensors. The blowing rate was defined as the pressure ratio $p_{0,b}/p_b$ where $p_{0,b}$ is the blowing air supply total pressure and p_b the base pressure measured without blowing. The optimum was determined by the observation of the pressure fluctuations measured at three angular positions on the model (0°, 40°, 80°) at two different free stream Mach numbers (0.4 and 0.55), (Figure 5).

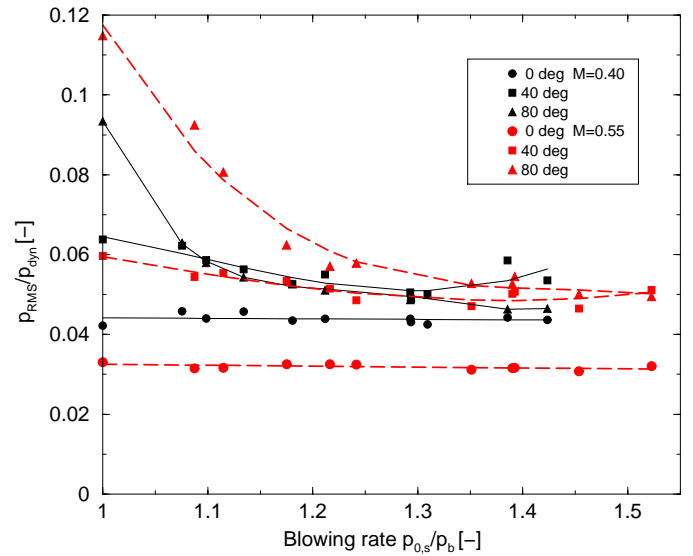Figure 5. *Effect of blowing rate on pressure fluctuations at 0°, 40° and 80° from experiments at Mach = 0.40 and 0.55.*

The results showed that the fluctuations decrease with increasing blowing rate until the air supply pressure equals the free stream total pressure. As already found from the numerical simulations, it was also seen that the measured time averaged pressure distribution is slightly affected when blowing, revealing the existence of a slightly higher acceleration on the front part of the model. The fluctuating pressure distribution (RMS) confirmed the numerical predictions as well, and an overall reduction of the pressure fluctuation amplitude could be observed up to the leading edge. The amplitude of the fundamental vortex shedding frequency is also strongly attenuated with blowing. It is clear from these conclusions that the gain in terms of reduction of dynamic errors on the unsteady angle will be even higher in the cases where vortex shedding lock-on is eliminated thanks to base bleed.

Probe Manufacturing and Instrumentation

The design in Figure 1 clearly demonstrates the complexity of the probe construction conditioned by the requirement of placing all three sensors in the same measurement plane. The

probe is therefore made by the assembly of a support piece for the total pressure sensor and a shell containing the yaw angle sensors into the probe stem. Due to their very small size, all pieces had to be manufactured by electro-erosion. This technique permitted the machining of small cavities housing the sensors and of non-circular shaped pressure holes. In order to limit the thermally induced stresses on the sensors, the probe material was chosen as Invar (64%Fe/36%Ni) which has the property of having basically no thermal expansion, while most alloys show thermal expansion coefficients two or three times higher than Silicium.

One major constraint in the assembly of the probe is the electrical insulation of the sensors with respect to the probe. This is performed by a thin layer of glue of ≈ 10 μm applied over the surface of the cavities. The sensors are then glued in their respective cavities using a two component epoxy resin and ball-stitch wire interconnections are done by ultrasonic bonding of very thin gold leads (Ø 40 μm) between the sensor bonding pads and thicker insulated copper leads of 70 μm diameter. The whole arrangement is then covered by glue to ensure stability and reliability of all connections (Figure 6).
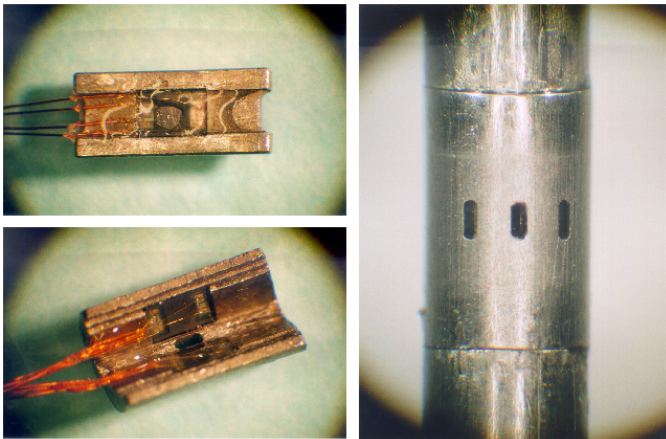

Figure 6. *AP3-H30. View of the sensors with their electrical connections glued inside their cavities (left) – View of the assembled probe head (right).*
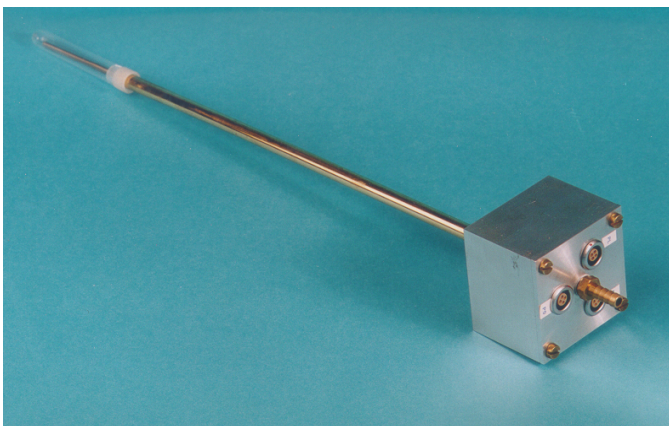

Figure 7. View of the AP3-H30 probe.

The probe head is then inserted into a Ø 8 mm stem made of

brass at the end of which a sealed connection box is fixed, housing the electrical connectors for the sensors as well as a pneumatic connection for the blowing air supply (Figure 7.).

The side surfaces of this connection box serve as reference planes for angular positioning and care was taken to reduce all misalignment errors with respect to the probe head by close fitting parts or one-to-one assemblies with tight tolerances.

Static Calibration

The static calibration of the probe is performed as a function of pressure and temperature by inserting the probe head in a sealed chamber, which is immersed into a thermostatic oil bath. Pressure variations are recorded at several temperature levels after thermal equilibrium is reached.

A traditional way of modelling the calibration data is to perform linear regressions on the bridge output variations versus pressure at each temperature level. The evolution of sensitivity and offset as a function of temperature then allows to define a reference sensitivity S_0 and offset O_0 at ambient temperature (20ºC) as well as their rate of change versus temperature dS/dT and dO/dT. The corrected pressure is then recalculated according to the following equation :

$$P = \frac{1}{S_0 + \frac{dS}{dT}(T-T_0)} \cdot \left[V_p - \left[O_0 + \frac{dO}{dT}(T-T_0) \right] \right]$$

This method assumes a linear dependence of sensitivity and offset to temperature. This assumption can turn out to be wrong in cases where all bridge resistors of the sensor do not have the same temperature coefficient of resistance or if mechanical stresses are induced by the changing characteristics of the glue used for sensor bonding. Moreover, the sense voltage is also generally assumed to change linearly with temperature. The same procedure applied to the sense voltage variations versus temperature at each pressure level shows high non-linearities of the slope and origin of V_{sense} versus pressure. This means that bridge output voltage and sense voltage are both a function of pressure *and* temperature. Pressure (and temperature) can be plotted directly versus the bridge output voltage V_p and the sense voltage V_{sense} and the errors arising from these non-linearities can be avoided by using direct interpolation in the calibration maps (Figure 8). This method avoids approximations linked to any kind of modelling of calibration data, reduces the complexity of calculations and improves remarkably the accuracy.

Regarding the achievable long term DC accuracy of pressure measurements, a simple pre-test calibration at some reference pressures is recommended in order to evaluate eventual drifts while temperature dependence can be assumed constant. Dénos & Valenti, 2000, proposed a method to determine the calibration coefficients by an optimization routine fitting the sensor pressure to a pneumatic probe recording. They also demonstrated that the response of semiconductor sensors can be strongly altered by fast temperature transients and developed a correction method based on the rate of change of the sense voltage versus temperature.
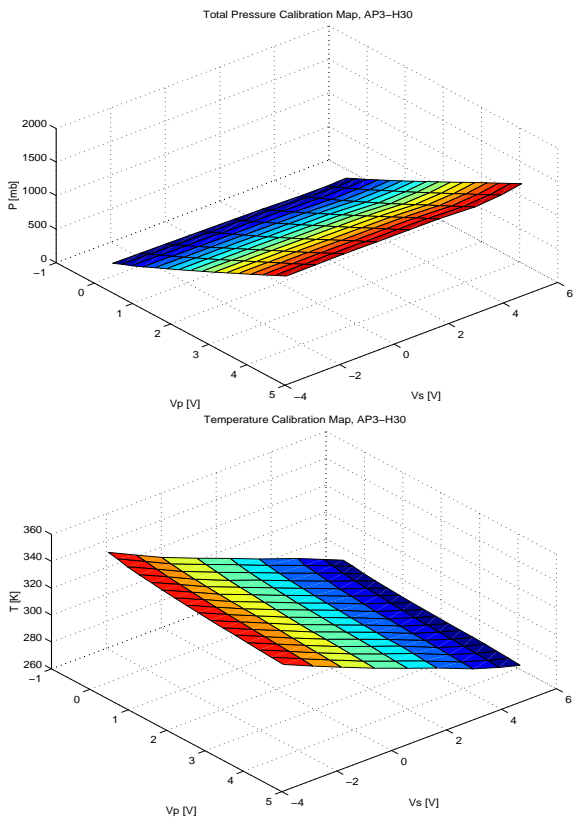
Figure 8. *Pressure and temperature calibration maps for the total pressure sensor of the AP3-H30 probe.*

Aerodynamic Calibration

After the static calibration of the sensors versus pressure and temperature, the second step towards the complete description of the relationship between the probe voltage outputs and the investigated flow quantities is the aerodynamic calibration of the probe in a reference flow.
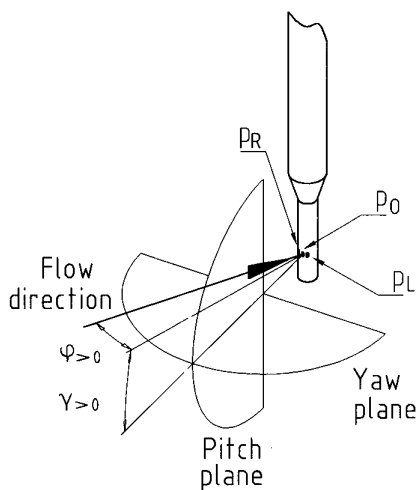

Figure 9. *Reference for positive pitch (γ) and yaw(φ) angles.*

The AP3-H30 probe was calibrated in the vertical-nozzle free jet facility (Ø 100 mm) of the ETH Zürich Turbomachinery Lab (Kupferschmied & Gossweiler, 1992). Although the probe

is essentially two-dimensional, the angular calibration was performed both in pitch and yaw angles respectively from +15º to –15º and from +40º to –40º, at 3 different Mach numbers (0.2, 0.4, 0.6). The corresponding angular references are presented in Figure 9.
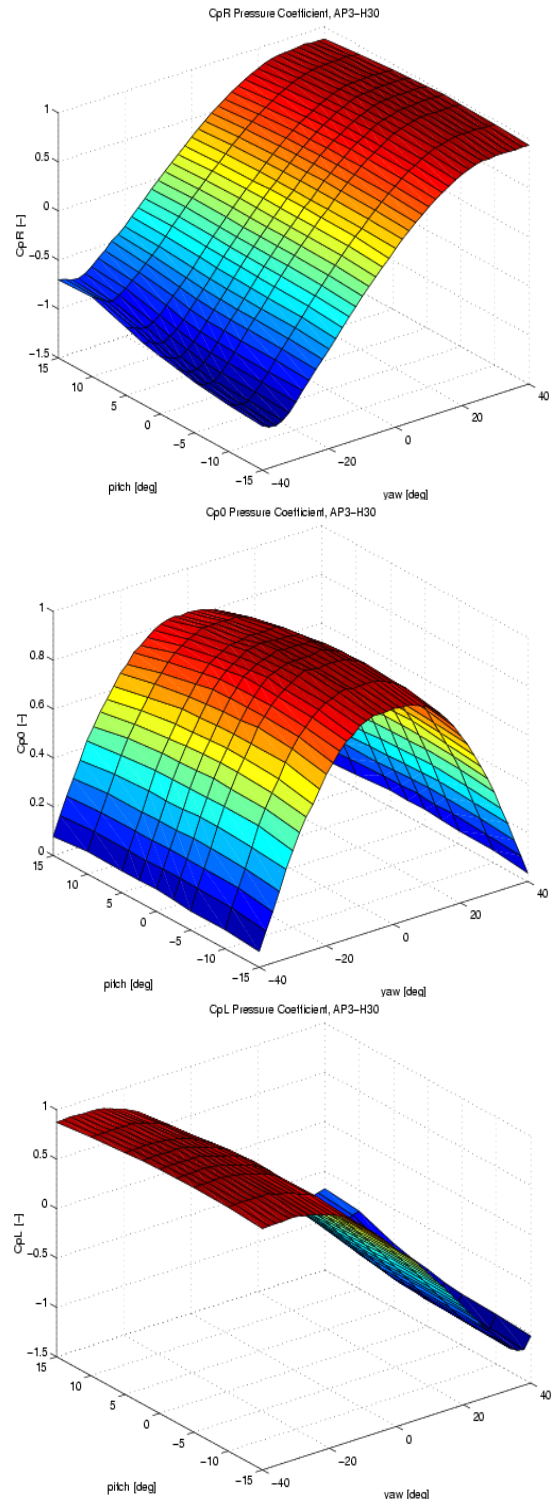

Figure 10. *Typical non-dimensional pressure coefficients for all 3 sensors of the AP3-H30 probe, Ma=0.6.*

The typical non-dimensional pressure coefficients C_p obtained for each sensor are presented in Figure 10 at Mach=0.6. The surfaces represent the typical pressure distribution around a cylinder.

Figure 11 represents the evolution of each coefficient versus yaw angle at three pitch angle values (-15º, 0º, +15º). The effect of pitch angle variations on all coefficients was found to be small, increasing however for positive pitch angles. This effect, related to the stem blockage effect, is visible for all coefficients and even more clearly at extreme yaw angles (+40º or –40º) for the yaw sensors.

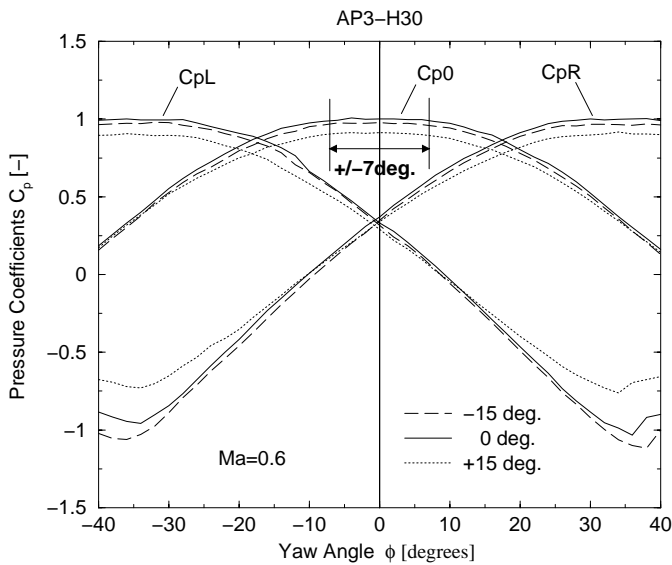Total pressure was found to be insensitive to yaw variations (within 1%) in an angular range of ± 7º.

Figure 11. *Pressure coefficients versus yaw angle at -15º, 0º, +15º pitch angles for all 3 sensors of the AP3-H30 probe, Ma=0.6.*

In normal operation of the probe, the air supply for base bleed was controlled with a pressure regulator and adjusted to the free stream total pressure. However, an additional calibration was performed at Mach = 0.4 without base bleed in order to assess its influence on the steady state angular characteristics of the probe. The results showed basically no substantial difference between the two sets of curves for any of the sensors. This can be explained with the help of Figure 3, in which the same comparison from numerical simulations shows very little difference as well, particularly in the 0 to 80º range. Similar conclusions were drawn already after the wind tunnel experiments on blowing rate.

Data Reduction Method

In order to evaluate the physical flow quantities from the pressure readings, an appropriate set of aerodynamic calibration coefficients has to be defined. These non-dimensional coefficients are all functions of Mach number as well as pitch and yaw angle. Yaw angle, total pressure and static pressure sensitivities are based on the probe dynamic pressure and can be expressed as follows :

$$K_\phi = \frac{P_L - P_R}{P_0 - \dfrac{P_L + P_R}{2}}$$

$$K_{tot} = \frac{P_T - P_0}{P_0 - \dfrac{P_L + P_R}{2}} \qquad K_{dyn} = \frac{P_T - P_S}{P_0 - \dfrac{P_L + P_R}{2}}$$

As the flow Mach number is generally unknown, a fourth coefficient can be defined as Mach sensitivity :

$$K_M = \frac{P_0}{P_0 - \dfrac{P_L + P_R}{2}}$$

Since the probe is essentially two-dimensional, an assumption has to be made about the pitch angle : either its average value is known from other measurements and the corresponding calibration surfaces can be derived, or it is unknown and assumed to be zero by default. All coefficients were therefore computed and plotted at zero pitch angle versus yaw angle and Mach number. The corresponding surfaces are presented in Figure 12.

In order to determine the unknown flow quantities, a direct method can be used. The knowledge of $K\varphi$ and K_M allows to compute the values of yaw angle and Mach number.

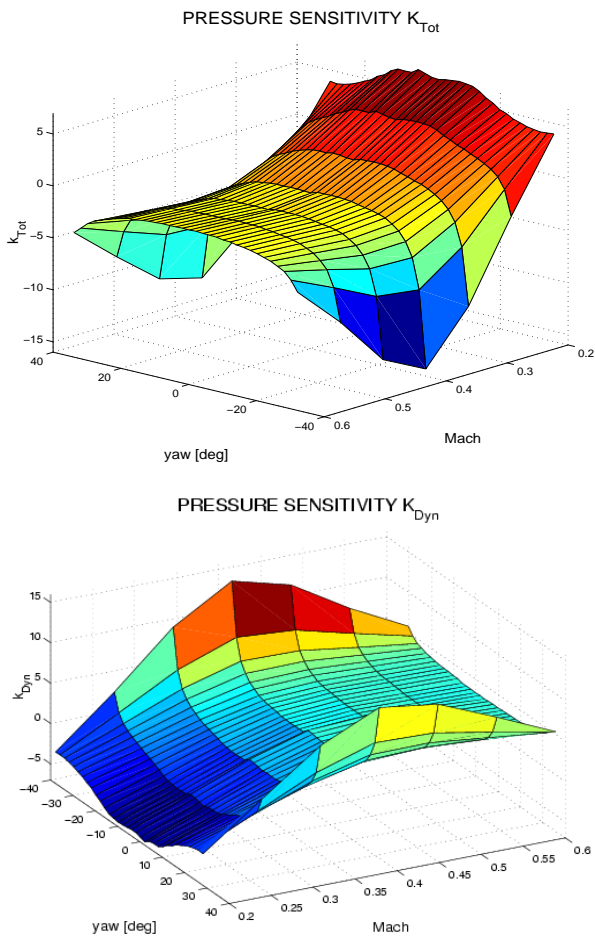ANGULAR SENSITIVITY K_{yaw}

MACH SENSITIVITY K_{Mach}
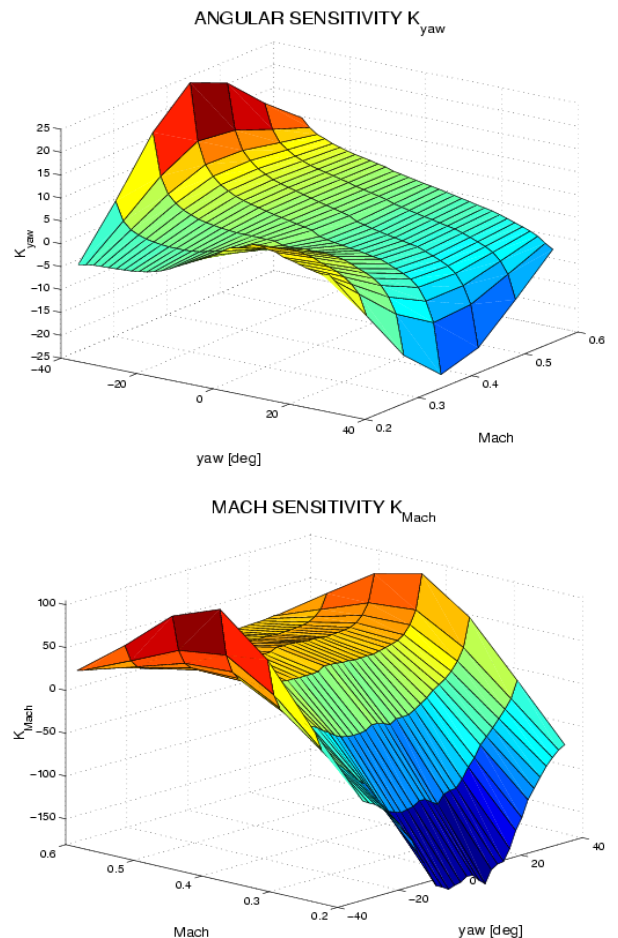
Figure 12. *Calibration surfaces of the AP3-H30 probe at Ma=0.6.*

The values of K_{tot} and K_{dyn} are then found by interpolation in the corresponding surfaces and the true values of the free stream total pressure p_T and static pressure p_S can be calculated.

As it can be noticed from Figure 12, the calibration surfaces present some "irregularities" at the boundaries of the angular domain. These strong gradients are due to the fact that all coefficients are based on the probe measured dynamic pressure which looses proportionality to the true dynamic pressure at large angular positions with respect to the mean flow. The value of the denominator shows numerical poles at large angles, which is a limit for the angular range in which the data can be evaluated.

To overcome this problem, in case large angular fluctuations are expected, all aerodynamic coefficients can be defined on the basis of the true dynamic pressure (p_T-p_S) as proposed by Contini et al., 1998. The procedure however becomes iterative, starting with a first guess of the dynamic pressure taken from the pressure readings until convergence on the Mach number.

Dynamic Calibration

The last step in the calibration process of a fast response

aerodynamic probe is the determination of its dynamic behavior.

As already mentioned above, the response of the pressure signal broadly depends on the dynamic properties of the sensor diaphragm and its distance to the source of pressure fluctuations.

Shock Tube Experiments

After the optimization process on the tap length and diameter with the help of the line-cavity theory of Bergh & Tijdeman, 1965, the experimental characterization of the probe dynamic response was carried out in the shock tube of ONERA IMFL in Lille (Sudan & Flodrops, 1981). Tests were performed at two different Mach numbers (~1.20 and ~1.40) at which the generated pressure step is the closest to a theoretical step function. The signals from the flush-mounted reference transducer and from the probe both inserted in the shock tube end plate were recorded simultaneously at a sampling frequency of 5 MHz. An example of recorded signals is shown in Figure 13 in terms of normalized pressures for the total pressure transducer of the probe.
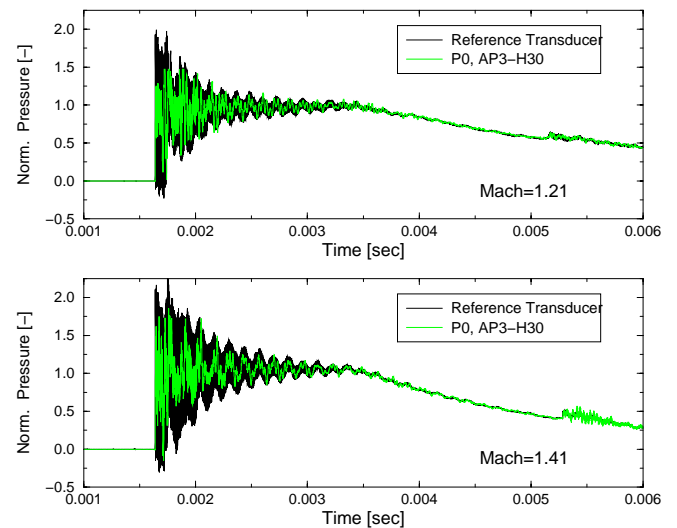

Figure 13. *AP3-H30. Comparison of the normalized pressure signals from shock tube experiments at different Mach numbers (fs=5 MHz).*

The effect of the pressure tap cavity is already clearly visible when comparing the attenuation of the probe pressure fluctuations to the reference signal after the shock wave reaches the end plate.

The goal of the data reduction is then twofold : first, the natural resonance frequencies of the pressure tap cavity and the sensor diaphragms should be isolated and second, a transfer function should be possibly determined in order to apply a frequency compensation to the slowest measurement systems. The signal processing method used is explained in the following.

Signal Processing

Both reference and probe signals are first preconditioned for Fast Fourier transformation by removing the initial constant

8

pressure level as well as the end part of the signal so as to keep a number of points equal to a power of 2. The processing method then consists of calculating the amplitude ratio of both frequency spectra in order to obtain a "raw" transfer function. The resulting spectrum appears very "noisy" due to the division in some points of small amplitudes present in both original spectra. An exponential smoothing is then applied forward and backward (to avoid phase distortion) on the "raw" transfer function, which is sufficient to remove uncorrelated peaks. The adjustment of the smoothing factor is done until a clear resonance frequency can be distinguished in the expected frequency range of cavity resonance. The transfer functions obtained in this way are presented in Figure 14 and compared to the theoretical prediction by the line-cavity theory.
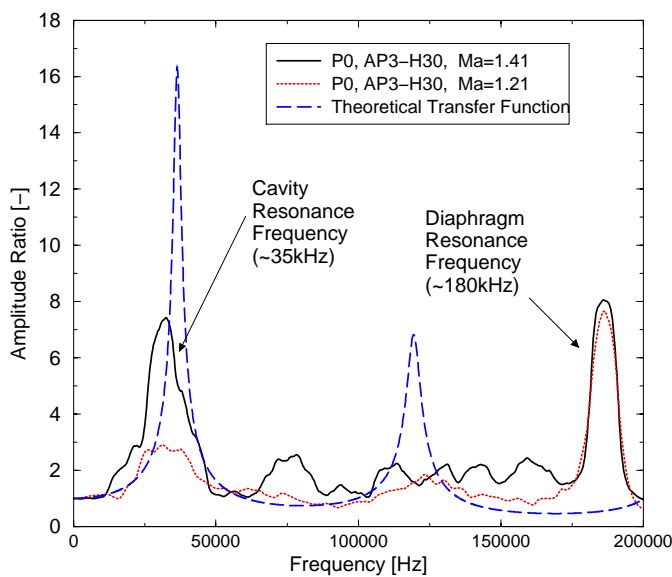

Figure 14. *Comparison of experimental and theoretical transfer functions from shock tube experiments, central transducer, AP3-H30.*

Both experimental transfer functions show clearly the natural frequency of the total pressure sensor at about 180 kHz whereas the theoretical model assumes an infinite frequency response of the sensor and predicts therefore only the cavity response. Although the theory of Bergh & Tijdeman assumes also large l/d ratios, small pressure steps and laminar flow in the line, the agreement with the experiments turns out to be very satisfactory. The measured cavity resonances both indicate a 35 kHz frequency against a theoretical frequency of 42 kHz. Still, the peak amplitude seems to be dependent on the shock Mach number, i.e. the magnitude of the pressure step and the odd harmonic of the theoretical second order system could not be identified in the measured transfer functions. The cavity resonances of the yaw sensors could similarly be identified around 75 kHz, while theory predicts 82 kHz. The measured transfer functions appear to be less dependent on Mach number which favours the hypothesis of non-repeatability between tests or irregularities in the bursting of the shock tube membrane.

These attempts to derive a transfer function by means of

frequency analysis of shock tube recordings show a good agreement between theory and experiments and suggests that the analytical transfer function could be used to better fit the experimental function and further on to apply frequency compensation.

SINGLE-SENSOR PROBES

Single-sensor probes are of course best suited to meet both requirements of space and time resolution. In order to achieve further miniaturization and higher dynamic response, the decision was taken to build a Ø 2.5 mm fast response probe (AP1-C25) combined with a Ø 0.3 mm pneumatic total pressure tap and a 12.5 μm half-shielded chromel-alumel thermocouple. This combination makes the probe very attractive for industrial applications in continuously running machines since it yields not only the accurate time-average and fluctuating component of the total pressure but also the time-averaged total temperature.
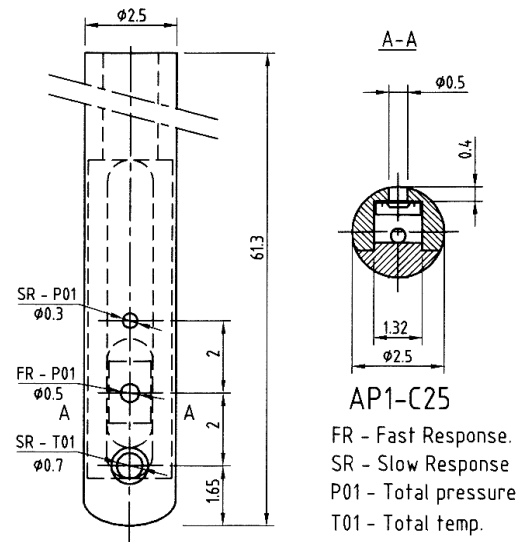

Figure 15. *The VKI AP1-C25 fast response combined pressure probe.*

The lower level of complexity of such a probe allows to turn back to conventional machining techniques, the micro-fabrication and packaging techniques still remaining a challenging task in the probe construction.

The probe material was therefore chosen as brass to avoid machining problems for this first probe and a fully cylindrical probe geometry was adopted. No base bleed was incorporated in the design since previous studies have shown a negligible influence on total pressure measurements on the contrary to the side ports measurements. The probe head extremity was rounded off to reduce three-dimensional effects. The sensors used are identical to the 15 Psi absolute sensors of the AP3-H30 probe. The pressure tap cavity was chosen as a circular hole of Ø 0.5 mm and length 0.4 mm which results in a theoretical frequency response of 127 kHz. The AP1-C25 probe (*Aerodynamic Probe* with *1 sensor*, *Circular* profile of Ø *2.5* mm) is presented in Figure 15.

The probe was calibrated aerodynamically under the same

conditions as described for the AP3-H30 probe. The dynamic response of the probe was not yet investigated experimentally, the predicted resonance frequency being sufficiently high to result in a large actual bandwidth.

Further Miniaturization

Further miniaturization could be achieved thanks to the availability of smaller sensors developed for biomedical applications at KUL (Katholieke Universiteit Leuven) in Belgium by Puers and De Bruycker (1998).
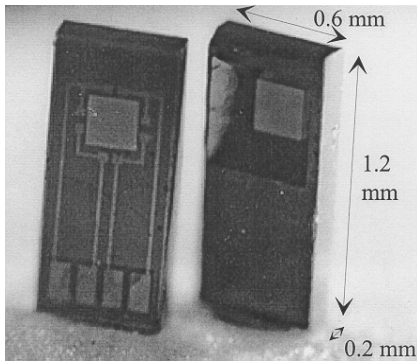

Figure 16. *10 Psi differential miniature piezoresistive pressure sensors developed at the Katholieke Universiteit Leuven, Belgium.*

Figure 17. *The VKI AP1-C15 miniature fast response pressure probe.*

The sensors are 10 Psi differential with a sensitivity of 5mV/V/bar (Figure 16). Like the absolute sensors previously described, they are powered at 5V DC by the same electronic circuit monitoring the sensor temperature. Their reduced dimensions (1.2mm x 0.6mm x 0.2mm) motivated the

manufacturing of a Ø 1.5 mm miniature single sensor probe (Figure 17) which can be looked at like a scaled-down version of the Ø 2.5 mm probe AP1-C25. While the pneumatic pressure hole (Ø 0.25 mm) was maintained as a check of the sensor steady state pressure, no space was available anymore for a thermocouple due to the smaller dimensions of the probe. The diameter of the fast response pressure tap was also reduced to 0.3 mm whereas the sensor can now be implemented only 0.25 mm underneath the cylinder surface. This length-to-diameter combination leads to an estimated frequency response of 110 kHz. This probe is the latest development in the fast response programme of the VKI Turbomachinery Lab, and is therefore not yet completely characterized, namely from an angular and dynamic point of view. The two above mentioned single-sensor probes are shown in Figure 18.
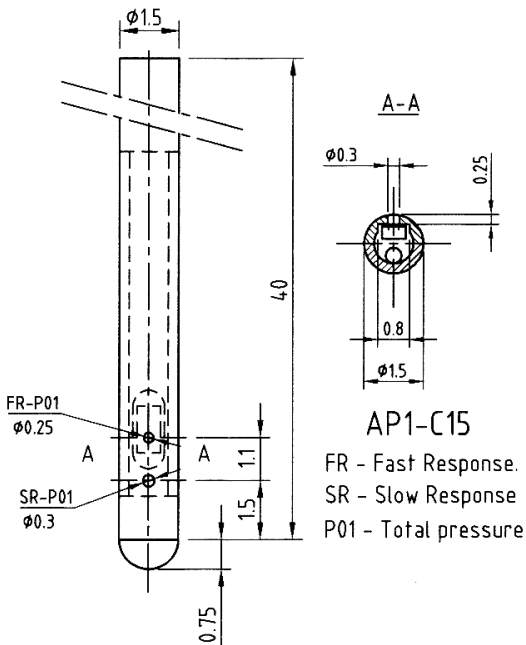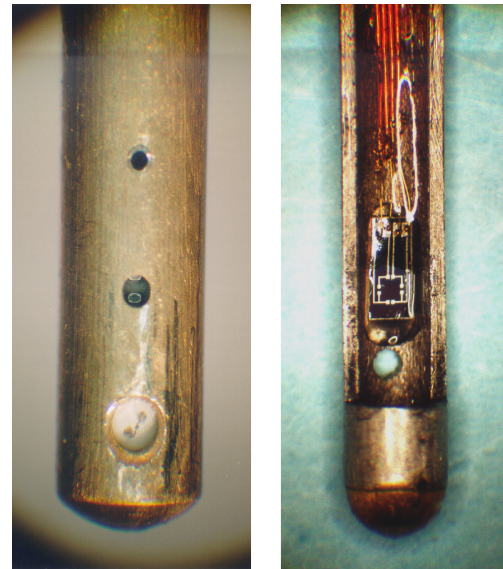

Figure 18. *View of the AP1-C25 probe head (left) and of the AP1-C15 probe under instrumentation (right).*

MEASUREMENTS

As a first application to turbomachinery flow field analysis, all three probes were used in the VKI blowdown turbine stage facility CT-3. The probes were inserted downstream of the transonic turbine stage at different pitchwise positions with respect to the stator.

A first series of tests was conducted in which only the 3-hole probe was used. The base bleed air supply was provided by a Pitot-type pipe of 4 mm inlet diameter to ensure a sufficient air massflow at a total pressure equal to the stage downstream total pressure. The connecting line was made as short as possible to avoid losses, the reference box at the end of the probe stem serving as a settling chamber.

A second series of tests was then performed with the two single sensor probes AP1-C25 and AP1-C15. The back-pressure for the relative sensor of the AP1-C15 probe was adjusted to the mean total pressure during the test.

All probes were set at an angular position corresponding to the theoretical rotor absolute outlet angle.

Unsteady Results

High-speed acquisition is taken during blowdown at a sampling frequency of 300 kHz. In order to obtain a good resolution of the time-resolved quantities to be recorded, the signals are first high-pass filtered at 100 Hz before being amplified with a gain of 10 and recorded on a 12 bit data acquisition system. At nominal speed (6500 RPM), the rotor blade passing frequency is 6.9 kHz, which leads to a resolution of 43.3 sampled points per period.

In order to avoid drift errors, conversion to pressure was performed by using calibration coefficients deduced from the optimization procedure on the pressure and temperature variations during a pre-test run-up, as described by Dénos and Valenti, 2000.

Frequency Analysis

Figure 19 represents the frequency spectrum obtained for the total pressure sensor of the AP3-H30 probe. The rotor blade passing frequency and its harmonics are clearly visible as well as two resonances in the range of 35 and 115 kHz.
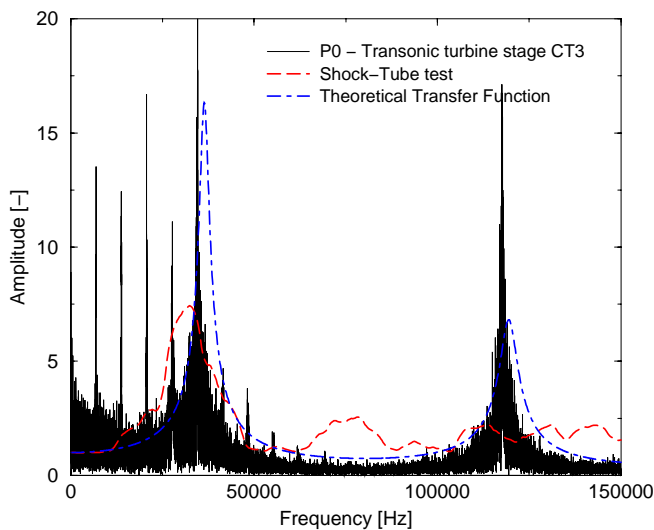

Figure 19. *Frequency spectrum of the AP3-H30 total pressure sensor compared to its theoretical and experimental transfer functions. $Re=1.10^6$, $P_{01}/P_{s3}=3.06$, 25% blade height.*

This result becomes even more interesting when superimposing the theoretical transfer function previously obtained. The almost perfect matching of the cavity resonance and its odd harmonic leads to the suggestion that the frequency spectrum could be used to adapt the amplitude and position of the peak resonances of the theoretical transfer function. Still, the frequency spectrum represents only the output of the transfer function for which the input remains unknown. These results are compared also to the experimental transfer function which shows also a good agreement. For these reasons, the inverse transfer function obtained from the shock tube experiments was used to perform the frequency compensation on the pressure signals. In order to eliminate the second resonance and in general to remove the high frequency noise, all signals were low-pass filtered at 60 kHz before compensation.

Phase-Locked Averaging

Regarding the mean fluctuations over one rotor pitch, a phase-locked average was applied to the pressure data. The averaging procedure was based on 3 full rotor revolutions, i.e. 192 blade passages, during which the increase of rotational speed is taken into account. The corresponding results are presented in Figure 20, comparing the phase-locked averaged signals before and after frequency compensation.
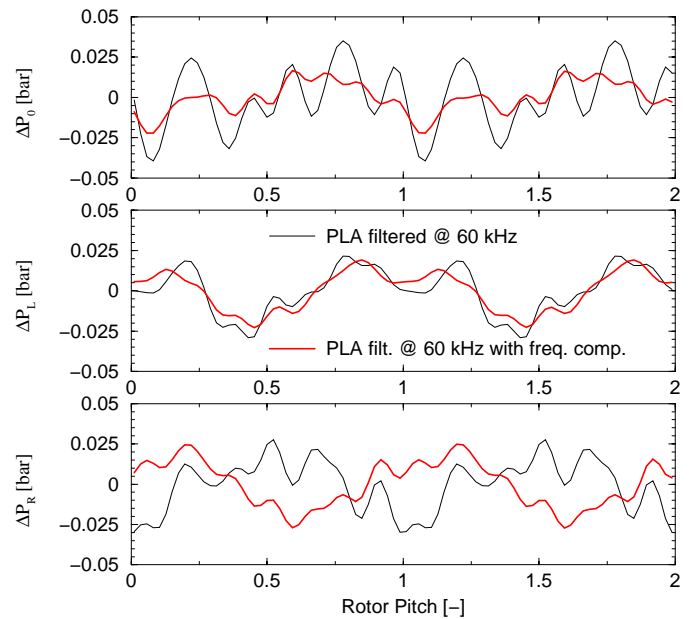

Figure 20. *Phase-locked averages of the AP3-H30 pressure signal before and after frequency compensation by the experimental transfer function.*

The large oscillations present mostly in the total pressure signal correspond to the third and fourth harmonics of the blade passing frequency that are overamplified by the cavity resonance. As it can be noticed from the comparison of the original signal with the compensated one, these fluctuations are now reduced. They correspond to 3% of the inlet total pressure.

Concerning flow field analysis, it is very difficult to comment these traces since there is no clear evidence about a distinguishable effect of the rotor wake neither in the left and right pressures nor in the total pressure. The analysis is further complicated by the presence of the following phenomena which influence the downstream total pressure : remaining secondary flows from the vane or the vane wake itself, secondary or tip leakage flows from the rotor or possible hub disk leakages. Downstream of the rotor, where the absolute outlet Mach number is subsonic (0.43), the correlation level of the phase-locked averages was found very poor (below 0.5). This indicates that the rotor downstream flow field is strongly affected by non-periodic phenomena in the subsonic range. This low correlation coefficient contrasts with that of pressure measurements between stator and rotor where the flow field is strongly dominated by the stator trailing edge shock, leading therefore to high correlation levels (~0.9).

The combination of the three phase-locked averaged pressure

traces then finally leads to the unsteady outlet angle shown in Figure 21, following the data reduction direct procedure described above.

Surprisingly, a very strong peak appears in the trace at 10% of the rotor pitch, which could be attributed to the wake. The angle variation in the wake is very high, which is a consequence of the strong velocity deficit on the exit velocity triangle. The corresponding total pressure loss is however difficult to identify in the phase-locked average without the help of the unsteady yaw angle trace. The small oscillations originally present in the total pressure can also be recognized in the unsteady angle in the core region of the flow (between 20 and 70% of the pitch).

A comparison of these preliminary results with numerical simulations would be very helpful in drawing some more explicit conclusions as regards the measurement technique and data reduction method as well as the flow field analysis.
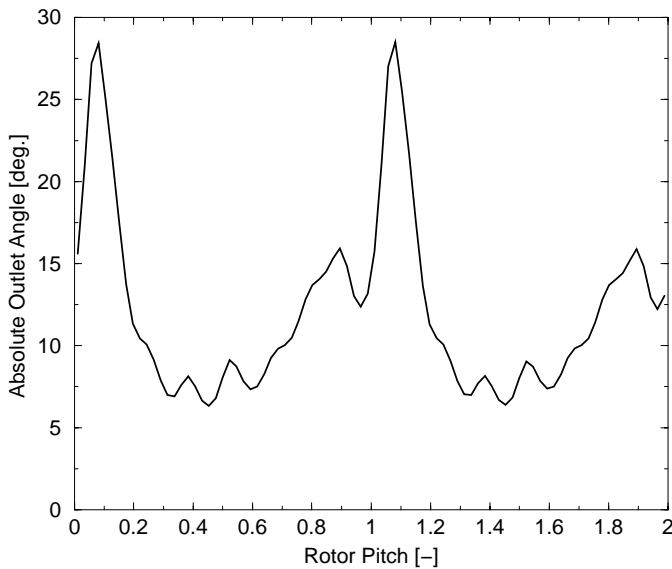

Figure 21. *Unsteady rotor absolute outlet angle as measured by the AP3-H30 probe. Re=1.10^6, P$_{01}$/P$_{s3}$=3.06, 25% blade height.*

Accuracy

Finally, regarding the accuracy of the steady and unsteady angles, the accuracy on pressure is evaluated to $\pm$ 1 mbar, which results in a $\pm$ 0.25 ° uncertainty on the angle. However, for large incidences, i.e. at the boundaries of the angular calibration domain, this value can amount to several degrees due to the steep gradients in the aerodynamic coefficients at these locations.

Total Pressure Measurements

The two single-sensor probes described above (AP1-C25 and AP1-C15) were used simultaneously to measure the rotor downstream total pressure. Their respective frequency spectra are presented in Figure 22 and again compared to the theoretical transfer functions. The cavity resonances are also visible at 150 kHz (AP1-C25) and 115 kHz (AP1-C15) but seem to be underestimated by the theory. In any case, as

previously mentioned, a cut-off frequency of 60 kHz was applied to filter the signals, leaving 6 or 7 harmonics in the frequency content for phase-locked averaging. No frequency compensation was applied in this range.
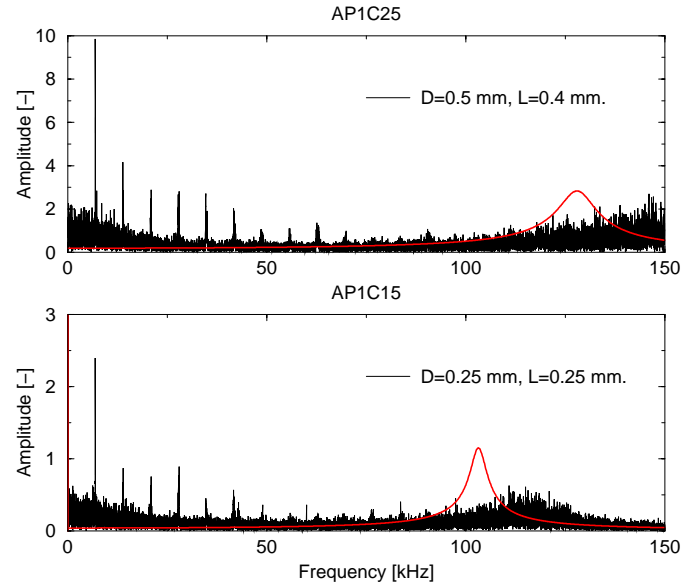

Figure 22. *Frequency spectra of the AP1-C25 and AP1-C15 probes. Comparison with their theoretical transfer functions.*

Since the probes were inserted at different azimuthal positions, the phase-locked averages were shifted in pitchwise direction with respect to each other to match the same reference with respect to the rotor. This allows the comparison in Figure 23 where a good agreement can be found between both signals. The differences, however, are to be attributed to the geometrical characteristics of each probe.
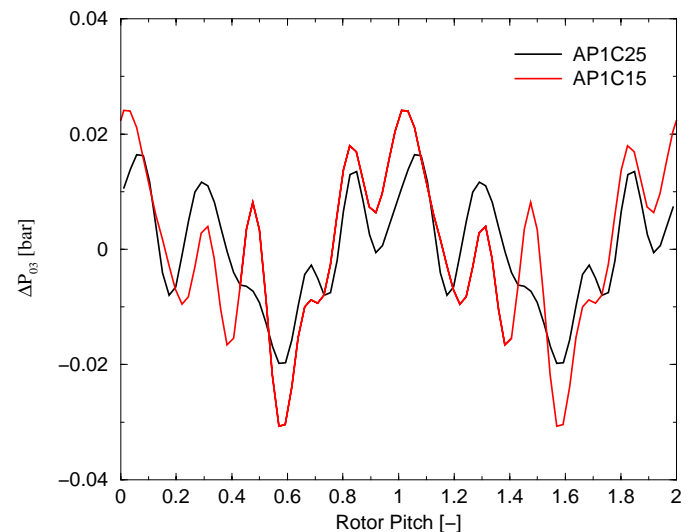

Figure 23. *Phase-locked averages of the downstream total pressure as measured by the AP1-C25 and AP1-C15 probes. Re=1.10^6, P$_{01}$/P$_{s3}$=3.06, 50% blade height.*

As a matter of fact, due to a smaller diameter and a better

spatial resolution, the AP1-C15 probe causes lower blockage and allows a better resolution of the pressure fluctuations. It should be recalled here that the rotor trailing edge thickness is 1.02 mm and measurements are taken at 0.50 $C_{r,ax}$ (19.7 mm) downstream of the rotor. The pressure hole (Ø 0.25 mm) is also half of the diameter of the AP1-C25 pressure hole. Total pressure is therefore integrated over a smaller angular range. All these factors justify the higher fluctuations picked up by the AP1-C15 probe and clearly show the advantages of probe miniaturization.

CONCLUSIONS

Fast response aerodynamic probes have become very helpful tools in flow field analysis and are particularly well suited for turbomachinery applications. Not only their robustness and reliability but also their ability to measure the steady and unsteady components of the flow vector as well as the time-resolved total and static pressure are precious qualities of this measurement technique.

Still, many different factors have to be taken into account in order to obtain accurate measurements. The development of a fast response three-hole probe and of two single-sensor probes described in this paper reflects these various considerations.

The requirements for accurate time-resolved measurements have led to the choice of cylindrical probes which combine good dynamic characteristics with a large calibration range suitable for data evaluation. Unsteady errors on the angle measurements due to vortex interactions have been reduced by the implementation of base bleed along the probe trailing edge.

A careful sensor calibration as well as an extensive aerodynamic calibration must be performed, and a subsequent data modelling must be adapted to reduce systematic errors.

Frequency compensation is sometimes mandatory and can be applied through a transfer function which can be obtained from shock tube experiments.

Finally, the preliminary results obtained in the very severe frame of blowdown experiments in a transonic turbine stage are very encouraging both from the point of view of accuracy and reliability.

AKNOWLEDGEMENTS

REFERENCES

- Ainsworth, R.W., Allen, J.L., Batt, J.J.M., 1994, "The development of fast response aerodynamic probes for flow measurements in turbomachines", ASME paper 94-GT-23.
- Ainsworth, R.W., Miller, R.J., Moss, R.W., Thorpe, S.J., 2000, "Unsteady Pressure Measurement", Meas. Sci. Technol. 11, pp 1055-1076.
- Bergh, H, & Tijdeman, H., 1965, "Theoretical and experimental results for the dynamic response of pressure measuring systems", NLR-TR-F.238.
- Brouckaert, J.F, Sieverding, C.H., Manna, M., 1998, "Development of a Fast Response Three-Hole Pressure Probe", Proceedings of XIVth Symposium on Measuring Techniques for Transonic and Supersonic Flows in Cascades and Turbomachines", Limerick, Ireland.
- Contini, D., Cortese, C., Manfrida, G., 1998, "Incertezza nella Misura del Vettore Velocita in un Flusso Tridimensionale con Sonda Pneumatica a 5 Fori", MIS-MAC V, Estratto degli Atti della Giornata di Studio, Roma.
- Dénos, R. & Valenti, E., 2000, "Influence of temperature transients and centrifugal force on fast response pressure transducers", Proceedings of XVth Symposium on Measuring Techniques for Transonic and Supersonic Flows in Cascades and Turbomachines", Firenze, Italy.
- Kupferschmied, P., Gossweiler, C.R., 1992, "Calibration, Modelling and Data Evaluation Procedures for Aerodynamic Multihole Pressure Probes on the Example of a Four Hole Probe", Proceedings of XIth Symposium on Measuring Techniques for Transonic and Supersonic Flows in Cascades and Turbomachines", Munich, Germany.
- Humm, H.J., Gizzi, W.P., Gyarmathy, G., 1994, "Dynamic response of aerodynamic probes in fluctuating 3-D flows", Proceedings of XIIth Symposium on Measuring Techniques for Transonic and Supersonic Flows in Cascades and Turbomachines", Prague.
- Kupferschmied, P., Koeppel, P., Gizzi, W., Roduner, C., Gyamarthy, G., 2000, "Time-Resolved Flow Measurements With Fast Response Aerodynamic Probes in Turbomachines", Meas. Sci. Technol. 11, pp 1036-1054.
- Manna, M., 1992, "A Three-Dimensional High Resolution Compressible Flow Solver", Ph.D. Thesis, Université Catholique de Louvain.
- Puers, R. and De Bruyker, D., K.U.Leuven, Electrical Engineering Department, Annual Report 1998, section 4.5.5: Silicon Bulk Micromachining, p.62.
- Richards, W.B., 1986, "Propagation of sound waves in tubes of non-circular cross section", NASA TP 2601.
- Sieverding, C.H. & Arts, T., 1992, "The VKI Compression Tube Annular Cascade Facility CT3", ASME paper 92-GT-336.
- Sieverding, C.H., Arts, T., Dénos, R., Brouckaert, J.F., 2000, "Measurement techniques for unsteady flows in turbomachines", Experiments in Fluids, Vol. 28 (Nr. 5), May 2000, presented at the IGTI conference Stockholm, 1998.